Modeling and Stability Analysis of Inertial Roll Coupling in Supersonic Sounding Rockets

Saptak Das*

Inertial roll coupling is a dynamic instability that can arise in slender, high-speed vehicles subjected to rapid roll motion, leading to unintended growth in pitch and yaw despite nominal aerodynamic stability. While the phenomenon has been studied historically in the context of early supersonic aircraft, it remains a relevant concern for modern sounding rockets and spin-stabilized launch vehicles operating in the transonic and supersonic regimes. This paper presents a compact dynamical model for inertial roll coupling based on rigid-body rotational dynamics and linear aerodynamic restoring moments. A coupled set of pitch–yaw equations is derived assuming a prescribed roll rate, and the resulting system is analyzed using state-space methods to assess stability as a function of roll rate. The analysis identifies a bounded roll-rate instability region in which small attitude perturbations can grow rapidly due to inertial coupling effects. Numerical simulations are used to illustrate the qualitative behavior of the system as the roll rate varies, emphasizing the role of roll magnitude and roll acceleration in determining stability. The proposed model and stability results are compared with classical inertial roll coupling formulations and analyses by Mandell, LaBudde, and Fetter, demonstrating consistency with established theory while offering a streamlined framework suitable for rapid analysis and design trade studies. This work directly supports ongoing flight dynamics analysis for the Georgia Tech Experimental Rocketry (GTXR), a project team of the Ramblin' Rocket Club (RRC) at the Georgia Institute of Technology, vehicle Mach 'N' Roll, a two-stage spin-stabilized sounding rocket scheduled to launch in summer 2026, and provides a foundation for future model extensions.

I. Nomenclature

$\alpha_x, \alpha_y, \alpha_z$	=	angle in the x, y, and z axes respectively
ω_z	=	angular velocity in the z (roll) axis
$\omega_p, \omega_y, \omega_r$	=	angular velocity in the pitch, yaw, and roll axes respectively
m	=	mass of the rocket
I_L, I_R	=	moment of inertia in the longitudinal and roll axes respectively
I_p, I_y, I_r	=	moment of inertia in the pitch, yaw, and roll axes respectively
M_{1y}	=	rotational forcing moment
M_{2y}	=	rotational damping moment
T_p, T_y	=	torque in the pitch and yaw axes respectively
k_p, k_y	=	aerodynamic stiffness in the pitch and yaw axes respectively
ρ	=	air density
v_T	=	velocity of the total oncoming airstream
A_r	=	reference area for the $C_{N\alpha}$. By convention, this is the cross-sectional area of the rocket body.
$C_{N\alpha}$	=	slope of the normal force coefficient vs angle of attack graph of the whole rocket
L_{CP}	=	distance from the nosetip to the center of pressure
L_{CG}	=	distance from the nosetip to the center of gravity
ω_n	=	undamped natural frequency
ω_d	=	damped natural frequency
ζ	=	damping ratio
C_1	=	rotational forcing coefficient

*Undergraduate Student, Daniel Guggenheim School of Aerospace Engineering, Georgia Institute of Technology, 620 Cherry Street NW, Atlanta GA 30332, AIAA Student Member, 1745275

C_2	=	rotational damping coefficient
C_3	=	x axis forcing coefficient
C_1'	=	coupled forcing coefficient
C_2'	=	coupled damping coefficient

II. Introduction

Inertial roll coupling is a dynamic instability that can occur in slender, high-speed rockets when roll motion induces gyroscopic interactions between pitch and yaw. Classical stability models developed by Mandell, LaBudde, and Fetter characterize rotational and translational dynamics but neglect direct pitch–yaw inertial coupling due to roll rate. For spin-stabilized sounding rockets operating in low-damping supersonic regimes, this coupling can produce a bounded roll-rate instability when roll rate approaches the vehicle's natural frequency. This work develops a coupled Roll Coupling Differential Equation (RCDE) model, analyzes its stability using eigenvalue methods, and compares its predictions to established formulations.

III. Literature Models

A. Derivation

The following derivation largely comes from Mandell's *Topics in Advanced Model Rocketry*, specifically Chapter 2: A unified approach to aerodynamic stability [1]. LaBudde and Fetter's derivations are largely based on Mandell's original derivation.

Define the rocket coordinate system such that the z-axis is aligned with the rocket's roll axis. The following equations describes a rocket's dynamic stability as derived from a 3D flight dynamics model. These equations leave out the jet damping moment since this has been shown to be negligible in comparison to the rotational damping. The $I_R\omega_z$ terms make the two equations coupled due to the non-zero roll rate. Thus, the pitch axis can be inertially coupled to the yaw axis by the presence of roll. Mandell's initial derivation disregards this coupling term.

$$I_L\frac{d^2\alpha_x}{dt^2} + M_{2x} + M_{1x} + I_R\omega_z\frac{d\alpha_y}{dt} = 0 \tag{1}$$

$$I_L\frac{d^2\alpha_y}{dt^2} + M_{2y} + M_{1y} - I_R\omega_z\frac{d\alpha_x}{dt} = 0 \tag{2}$$

Assuming small α and ω perturbations in the x and y axes, the rocket aerodynamics can be linearized like so:

$$\left.\frac{dM_1}{d\alpha}\right|_{\alpha=0} = \frac{\rho}{2}v_T^2 A_r C_{N\alpha}\left(L_{CP} - L_{CG}\right) \equiv C_1, \tag{3}$$

$$\left.\frac{dM_2}{d\alpha}\right|_{\alpha=0} = \frac{\rho}{2}v_T A_r C_{N\alpha}\left(L_{CP} - L_{CG}\right)^2 \equiv C_2. \tag{4}$$

Within the range of validity of the linearization approximation, the total applied moment about the x axis can be expressed as

$$M_x = -C_1\alpha_x - C_2\frac{d\alpha_x}{dt}. \tag{5}$$

Thus, Eqs. (1) and (2) with forcing functions $f_x(t)$ and $f_y(t)$ can be rewritten as

$$I_L\frac{d^2\alpha_x}{dt^2} + C_2\frac{d\alpha_x}{dt} + C_1\alpha_x + I_R\omega_z\frac{d\alpha_y}{dt} = f_x(t), \tag{6}$$

$$I_L\frac{d^2\alpha_y}{dt^2} + C_2\frac{d\alpha_y}{dt} + C_1\alpha_y - I_R\omega_z\frac{d\alpha_x}{dt} = f_y(t). \tag{7}$$

The homogeneous solution of the linear coupled second order differential equation system can be found by setting the forcing functions $f_x(t) = f_y(t) = 0$. For any arbitrary forcing functions, the resulting solution will be the sum of the homogeneous solution and a particular solution. Solving for the particular solution allows us to determine the exact impact of the forcing functions on the result.

B. Stability Analysis
The following stability analysis is based on Mandell's work. The implications of the coupling term will considered in Section III.C.

To solve for the homogeneous solution of Eqs. (6) and (7) at zero roll rate, apply the Laplace transform.

$$I_L s^2 \alpha_x + C_2 s \alpha_x + C_1 \alpha_x = 0 \tag{8}$$
$$I_L s^2 \alpha_y + C_2 s \alpha_y + C_1 \alpha_y = 0 \tag{9}$$

These equations can be transformed into a characteristic equation of the form:

$$I_L s^2 + C_2 s + C_1 = 0. \tag{10}$$

Then divide by I_L,

$$s^2 + \frac{C_2}{I_L} s + \frac{C_1}{I_L} = 0. \tag{11}$$

This system is the standard form of a second order linear system and thus the standard second-order parameters can be defined for model clarity.

$$\omega_n = \sqrt{\frac{C_1}{I_L}} \tag{12}$$
$$\zeta = \frac{C_2}{2\sqrt{I_L C_1}} \tag{13}$$

Then the characteristic equation becomes

$$s^2 + 2\zeta\omega_n s + \omega_n^2 = 0. \tag{14}$$

For most sounding rockets, the aerodynamic damping $\zeta < 1$, so the system is underdamped. Therefore, the roots of the characteristic equation are

$$s = -\zeta\omega_n \pm i\omega_d, \tag{15}$$
$$\omega_d = \omega_n\sqrt{1-\zeta^2}. \tag{16}$$

Taking the inverse Laplace form for these complex conjugate poles yields

$$\alpha(t) = e^{-\zeta\omega_n t}\left[A_1\cos(\omega_d t) + A_2\sin(\omega_d t)\right]. \tag{17}$$

The constants are determined from initial conditions

$$A_1 = \alpha(0), \tag{18}$$
$$A_2 = \frac{\dot{\alpha}(0) + \zeta\omega_n\alpha(0)}{\omega_d}. \tag{19}$$

Thus, the roll-plane rotational motion of the rocket is

$$\alpha_x(t) = e^{-\zeta\omega_n t}\left[\alpha_x(0)\cos(\omega_d t) + \frac{\dot{\alpha}_x(0) + \zeta\omega_n\alpha_x(0)}{\omega_d}\sin(\omega_d t)\right], \tag{20}$$
$$\alpha_y(t) = e^{-\zeta\omega_n t}\left[\alpha_y(0)\cos(\omega_d t) + \frac{\dot{\alpha}_y(0) + \zeta\omega_n\alpha_y(0)}{\omega_d}\sin(\omega_d t)\right]. \tag{21}$$

For slightly damped rockets ($\zeta \ll 1$), the motion is nearly harmonic with a slowly decaying amplitude.

C. Extensions to Stability Analysis

In Section III.B, the coupling term was ignored to simplify the calculation similar to Mandell's original derivation. Thus, Mandell's model assumes that the pitch and yaw axis rotational motions are independent of one another. Mandell's model also assumes that the rocket's center of gravity follows a straight-line trajectory regardless of rotation. This model predicts a damping ratio $\zeta \approx 0.01$, which implies that a rocket would oscillate for a long time (50+ cycles) before stabilizing.

Both LaBudde and Fetter assume that the rocket's center of gravity trajectory is not a straight line, but includes lateral motion [2, 3]. Fetter's analysis shows the damping ratio ζ is actually closer to 0.05, meaning the rocket stabilizes in only 5–10 cycles, which matches real-world observations.

In Mandell's model, the normal forces are responsible only for the restoring moment that causes the rocket to point into the wind. However, the normal forces also cause the entire rocket to move sideways. Fetter explains that as the rocket rotates, the normal forces push the CG sideways. This lateral velocity then changes the direction of the oncoming air relative to the rocket, effectively increasing the damping of the rotation. Fig. 1 shows the rocket dynamics due to the rotational dynamics and the lateral movement of the rocket due to an initial small angle of attack perturbation.

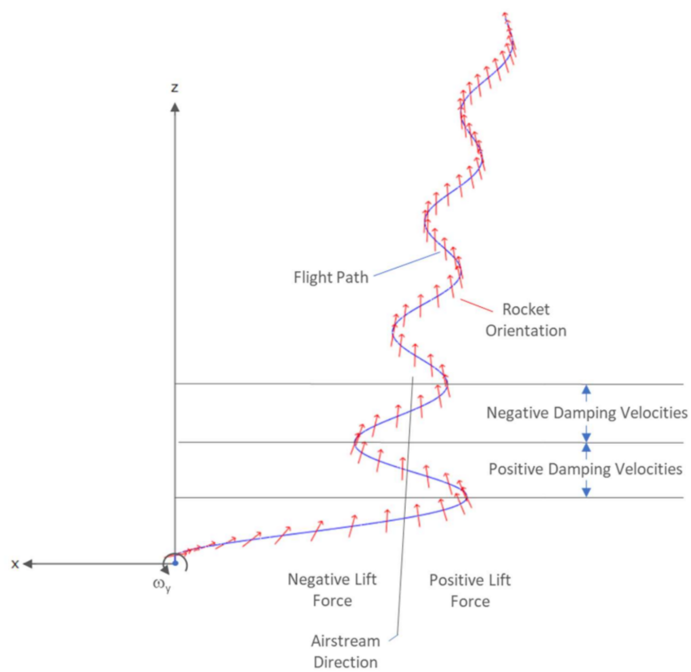

Fig. 1 Rocket response due to the rotational dynamics and the lateral movement of the rocket due to an initial small angle of attack perturbation. Motion in the x-axis is exaggerated by 1000x compared to the z-axis and the arrow attitudes are 10x α_y [3].

In his paper, Fetter argues that the traditional stability margin is not a good indicator of dynamic stability. His sensitivity analysis shows that increasing the stability margin can sometimes decrease the coupled damping ratio if the design change simultaneously reduces the rocket's ability to move side-to-side.

LaBudde and Fetter's analyses are quite similar. LaBudde introduces the impact of the coupling term in his paper since the primary focus of his paper is rocket altitude optimization. In comparison, Fetter focuses on validating the side-to-side motion using accelerometer flight data and root locus techniques to show how rapidly a rocket transitions from dynamically stable to unstable as design parameters change.

The below summary shows the differences between the three models for calculating the coupled natural frequency and damping ratio. Both use Mandell's definition for C_1 and C_2 and a different definition of C_3. Even though LaBudde and Fetter use different nomenclature, once both sets of expressions are evaluated in terms of the rocket parameters, the expressions for the linear and rotational dynamics coupled natural frequency and damping ratios are the same between LaBudde and Fetter's models. Note that LaBudde and Fetter still neglect the pitch-yaw coupling term like Mandell and thus pitch and yaw rotational motion are considered to be independent of one another. The derivation of these coupled natural frequency and damping ratio equations will not be discussed in this paper.

Mandell/Barrowman Uncoupled:

$$C_1 \equiv \frac{\rho}{2} v_T^2 A_r C_{N\alpha} \left(L_{CP} - L_{CG}\right) \tag{22}$$

$$C_2 \equiv \frac{\rho}{2} v_T A_r C_{N\alpha} \left(L_{CP} - L_{CG}\right)^2 \tag{23}$$

$$\omega_n = \sqrt{\frac{C_1}{I_L}} \tag{24}$$

$$= \sqrt{\frac{\rho v_T^2 A_r C_{N\alpha} \left(L_{CP} - L_{CG}\right)}{2 I_L}} \tag{25}$$

$$\zeta = \frac{C_2}{2\sqrt{I_L C_1}} \tag{26}$$

$$= \sqrt{\frac{\rho A_r C_{N\alpha} \left(L_{CP} - L_{CG}\right)^3}{8 I_L}} \tag{27}$$

LaBudde Coupled:

$$C_3 \equiv \frac{\rho v_T A_r C_{N\alpha}}{2m} \tag{28}$$

$$\omega_n = \sqrt{\frac{C_1 + C_2 + C_3}{I_L}} \tag{29}$$

$$= \sqrt{\frac{\rho v_T^2 A_r C_{N\alpha} \left(L_{CP} - L_{CG}\right) \left(\rho \left(A_r C_{N\alpha} L_{CP} - A_r C_{N\alpha} L_{CG}\right) + 2m\right)}{4 m I_L}} \tag{30}$$

$$\zeta = \frac{C_2 + C_3 I_L}{2\sqrt{I_L \left(C_1 + C_2 + C_3\right)}} \tag{31}$$

$$= \sqrt{\frac{\rho A_r C_{N\alpha} \left(m \left(L_{CP}^2 - 2 L_{CP} L_{CG} + L_{CG}^2\right) + I_L\right)^2}{4 m I_L \left(L_{CP} - L_{CG}\right) \left(\rho \left(A_r C_{N\alpha} L_{CP} - A_r C_{N\alpha} L_{CG}\right) + 2m\right)}} \tag{32}$$

Fetter Coupled:

$$C_3 \equiv \frac{\rho}{2} v_T^2 A_r C_{N\alpha} \tag{33}$$

$$C_1' = C_1 + \frac{C_2 C_3}{v_T m} \tag{34}$$

$$C_2' = C_2 + \frac{I_L C_3}{v_T m} \tag{35}$$

$$\omega_n = \sqrt{\frac{C_1'}{I_L}} \tag{36}$$

$$= \sqrt{\frac{\rho v_T^2 A_r C_{N\alpha} \left(L_{CP} - L_{CG}\right) \left(\rho \left(A_r C_{N\alpha} L_{CP} - A_r C_{N\alpha} L_{CG}\right) + 2m\right)}{4 m I_L}} \tag{37}$$

$$\zeta = \frac{C_2'}{2\sqrt{I_L C_1'}} \tag{38}$$

$$= \sqrt{\frac{\rho A_r C_{N\alpha} \left(m \left(L_{CP}^2 - 2 L_{CP} L_{CG} + L_{CG}^2\right) + I_L\right)^2}{4 m I_L \left(L_{CP} - L_{CG}\right) \left(\rho \left(A_r C_{N\alpha} L_{CP} - A_r C_{N\alpha} L_{CG}\right) + 2m\right)}} \tag{39}$$

D. Implications for Roll Coupling Modeling

The pitch-yaw dynamics derived above are mathematically identical to a classical second–order system. Writing the Laplace-domain transfer function from a forcing moment $F(s)$ to the angular response $\hat{\alpha}(s)$ gives

$$G(s) = \frac{\hat{\alpha}(s)}{F(s)} = \frac{1/I_L}{s^2 + 2\zeta\omega_n s + \omega_n^2}. \tag{40}$$

The frequency response (gain function) is obtained by evaluating $G(s)$ at $s = i\omega$.

$$|G(i\omega)| = \frac{1/I_L}{\sqrt{\left(\omega_n^2 - \omega^2\right)^2 + (2\zeta\omega_n\omega)^2}} \tag{41}$$

This expression reveals several important physical implications:

- For very low frequencies ($\omega \ll \omega_n$), the gain approaches $1/(I_L\omega_n^2) = 1/C_1$. The rocket behaves quasi-statically with the aerodynamic forcing moment dominating the response.
- Near $\omega \approx \omega_n$, the denominator becomes small and a resonant peak appears. For lightly damped systems, the height of this peak is approximated by
$$|G|_{\max} \approx \frac{1}{2\zeta I_L \omega_n^2}.$$
- Increasing ω_n shifts the resonance to a higher frequency and reduces the low-frequency gain. Physically, a lower-inertia rocket with larger aerodynamic forcing moments oscillates faster and resists low-frequency disturbances more strongly.
- Increasing ζ reduces the peak gain and broadens the frequency response. Thus, greater aerodynamic damping directly suppresses oscillatory amplification.

For sounding rockets where $\zeta \ll 1$, the gain curve exhibits a sharp resonance near ω_n. This explains why small periodic disturbances near the natural frequency can produce large coning motions if damping is insufficient.

Suppose that a rocket is being spin stabilized such that the roll rate ω_r is non-zero. In this case, the $I_R\omega_r$ coupling terms in Eqs. (6) and (7) introduce gyroscopic coupling between pitch and yaw. The system is no longer two independent second–order oscillators, but instead becomes a coupled fourth–order system with split modal frequencies.

Qualitatively, the effect of spin stabilization depends on the ratio of roll rate to natural frequency:

- **$\omega_r \ll \omega_n$:** The roll rate is slow compared to the pitch-yaw oscillation. Coupling is weak and the system behaves approximately like the uncoupled case. Spin provides little additional stabilization.
- **$\omega_r \approx \omega_n$:** Strong modal interaction occurs. The roll motion can parametrically excite the pitch/yaw oscillation based on the coupling term. In other words, an initial disturbance in the pitch axis is directly turned into a disturbance in the yaw axis in a strong positive feedback loop.
- **$\omega_r \gg \omega_n$:** The system approaches classical gyroscopic stabilization. Rapid spin averages aerodynamic disturbances over one roll cycle, effectively increasing directional stiffness. The pitch-yaw motion becomes slower relative to roll and typically more stable, provided structural and inertial asymmetries are small.

Physically, a high roll rate introduces gyroscopic stiffness proportional to $I_R\omega_r$. This modifies the effective natural frequencies of the lateral modes and can reduce sensitivity to crosswinds and thrust misalignment. However, an excessive roll rate may also introduce significant structural loads. Therefore, evaluating ω_r/ω_n provides a useful non-dimensional parameter for assessing whether a rocket behaves as weakly spinning, resonantly coupled, or strongly gyroscopically stabilized.

IV. Roll Coupling Differential Equation Model (RCDE)

A. Derivation

All the literature models above neglect the pitch-yaw coupling terms so that pitch and yaw rotational motion can be independently considered. However, for spin-stabilized rockets, the coupling between the pitch and yaw motion is significant to understanding the inertial roll coupling phenomenon. This model focuses on the effect of pitch-yaw coupling. Starting off with Euler's rotation equations, we will assume the angular rate of roll is controlled. Thus, the other rotations must satisfy

$$I_y\dot{\omega}_y = (I_p - I_r)\omega_r\omega_p + T_y, \tag{42}$$
$$I_p\dot{\omega}_p = -(I_y - I_r)\omega_r\omega_y + T_p. \tag{43}$$

At small angles of attack, the aerodynamic torques T_y and T_p are proportional to the vehicle's angular orientation θ_y and θ_p to the freestream air respectively. This torque model considers only the aerodynamic forcing torque since the aerodynamic forcing torque is small in comparison.

$$T_y = -k_y I_y\theta_y \tag{44}$$
$$T_p = -k_p I_p\theta_p \tag{45}$$

In the case of a rolling vehicle, the connection between orientation and angular velocity is not entirely straightforward, because the aircraft is a rotating reference frame. The roll inherently exchanges yaw for pitch and vice-versa.

$$\dot{\theta}_y = \omega_y + \omega_r\theta_p \tag{46}$$
$$\dot{\theta}_p = \omega_p - \omega_r\theta_y \tag{47}$$

To derive expressions for $\dot{\omega}_y$ and $\dot{\omega}_p$, take the time derivative of Eqs. (46) and (47).

$$\dot{\omega}_y = \ddot{\theta}_y - \dot{\omega}_r\theta_p - \omega_r\dot{\theta}_p \tag{48}$$
$$\dot{\omega}_p = \ddot{\theta}_p + \dot{\omega}_r\theta_y + \omega_r\dot{\theta}_y \tag{49}$$

Rearranging Eq. (47) into $\omega_p = \dot{\theta}_p + \omega_r\theta_y$, substituting it along with Eqs. (44) and (48) into Eq. (42) and simplifying.

$$I_y(\ddot{\theta}_y - \dot{\omega}_r\theta_p - \omega_r\dot{\theta}_p) = (I_p - I_r)(\dot{\theta}_p + \omega_r\theta_y)\omega_r - k_y I_y\theta_y \tag{50}$$
$$I_y\ddot{\theta}_y = I_y\dot{\omega}_r\theta_p + (I_p + I_y - I_r)\omega_r\dot{\theta}_p + \left((I_p - I_r)\omega_r^2 - k_y I_y\right)\theta_y \tag{51}$$

Similarly, rearranging Eq. (46) into $\omega_y = \dot{\theta}_y - \omega_r\theta_p$, substituting it along with Eqs. (45) and (49) into Eq. (43), and simplifying.

$$I_p(\ddot{\theta}_p + \dot{\omega}_r\theta_y + \omega_r\dot{\theta}_y) = (I_r - I_y)(\dot{\theta}_y - \omega_r\theta_p) - k_p I_p\theta_p \tag{52}$$
$$I_p\ddot{\theta_p} = -I_p\dot{\omega}_r\theta_y - (I_p + I_y - I_r)\omega_r\dot{\theta_y} + \left((I_y - I_r)\omega_r^2 - k_p I_p\right)\theta_p \tag{53}$$

Thus, Eqs. (51) and (53) are ordinary differential equations to model inertial roll coupling given any function $\omega_r(t)$. Using a numerical integration scheme such as RK45, one can solve an IVP of the above fourth-order, linear DE system.

B. Stability Analysis

To analytically determine when the system becomes unstable, we can perform a linear stability analysis of the coupled DE system using Eqs. (51) and (53) derived earlier. To create a state-space model of the system, let us define

$$\boldsymbol{x} = \begin{pmatrix}\theta_y\\ \theta_p\\ \dot{\theta}_y\\ \dot{\theta}_p\end{pmatrix} \text{ so that } \dot{\boldsymbol{x}} = A\boldsymbol{x}. \tag{54}$$

To convert the second-order system to a first-order system, let us define $x_1 = \theta_y$, $x_2 = \theta_p$, $x_3 = \dot{\theta}_y$, and $x_4 = \dot{\theta}_p$. Thus, we can write the relationships between x_1, x_2, x_3, and x_4 like so

$$\dot{x}_1 = x_3, \tag{55}$$
$$\dot{x}_2 = x_4, \tag{56}$$
$$\dot{x}_3 = \dot{\omega}_r x_2 + \frac{(I_p - I_r)\omega_r + I_y\omega_r}{I_y}x_4 + \frac{(I_p - I_r)\omega_r^2 - k_y I_y}{I_y}x_1, \tag{57}$$
$$\dot{x}_4 = -\dot{\omega}_r x_1 - \frac{(I_y - I_r)\omega_r + I_p\omega_r}{I_p}x_3 + \frac{(I_y - I_r)\omega_r^2 - k_p I_p}{I_p}x_2. \tag{58}$$

Thus, the state-space matrix is

$$A = \begin{pmatrix} 0 & 0 & 1 & 0 \\ 0 & 0 & 0 & 1 \\ a_{31} & \dot{\omega}_r & 0 & a_{34} \\ -\dot{\omega}_r & a_{42} & a_{43} & 0 \end{pmatrix}, \tag{59}$$

$$a_{31} = \frac{(I_p - I_r)\omega_r^2 - k_y I_y}{I_y}, \quad a_{34} = \frac{(I_p + I_y - I_r)\omega_r}{I_y}, \tag{60}$$

$$a_{42} = \frac{(I_y - I_r)\omega_r^2 - k_p I_p}{I_p}, \quad a_{43} = -\frac{(I_p + I_y - I_r)\omega_r}{I_p}. \tag{61}$$

To determine the stability over a range of constant roll rates ω_r and thus $\dot{\omega}_r = 0$, we can determine how the eigenvalues change by treating the system as linear time invariant. Fig. 2 is an example plot of the poles of the system for varying ω_r. At $\omega_r = 0$, there are two eigenvalues and their conjugates that all lie on imaginary axis. As ω_r increases, one pair of eigenvalues converges at the origin, while the other pair diverges. At a critical roll frequency ω_{start}, the converging pair of eigenvalues move off the imaginary axis and instead move along the real axis. Since one of the eigenvalues has a positive real part, the system becomes unstable with the magnitude of the real part representing the degree of instability. The magnitude of the real part initially increases with increasing ω_r after ω_{start} and then decreases to zero at ω_{end}. Then, both eigenvalue pairs diverge from the origin traveling along the imaginary axis again. The roll coupling instability band occurs from $\omega_{start} \leq \omega_r \leq \omega_{end}$.

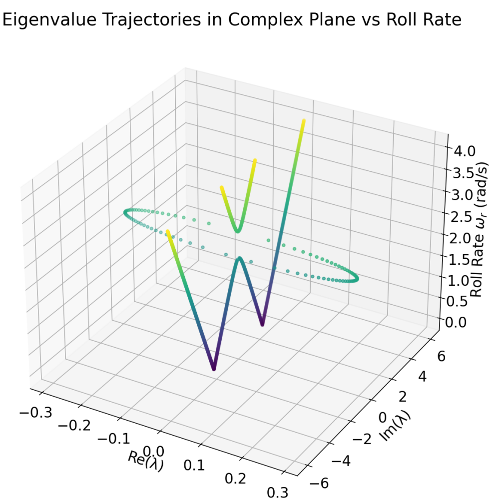

Fig. 2 Movement of System Poles for varying ω_r. The following parameters were arbitrarily used for this example: $I_y = 8.0$, $I_p = 10.2$, $I_r = 1$, $k_y = 5$, and $k_p = 5$.

Using this stability analysis, we can look at the effect of a ramping function $\omega_r(t)$. Fig. 3 shows the pitch and yaw behavior of the same system given a slow ramping function $\omega_r = 0.01t + 1$ through the roll coupling instability band determined previously. The system has an initial perturbation such that $\theta_y = 0.05$. The system is initially stable with only minor oscillations in the pitch and yaw due to the initial perturbation. However, once the system's roll rate enters the instability band, one can see the oscillations stop and the system starts to diverge. After 12 seconds, the vehicle would likely experience structural failure due to the aerodynamic forces at the steep angle of attack from the freestream direction. Even after the system's roll rate leaves the instability band, the pitch and yaw do not return to near zero angle of attack. Fig. 4 shows the pitch and yaw behavior of the same system given a fast ramping function $\omega_r = 0.04t$. In this case, the system stays in the instability band for about 15 seconds. Though the system had started to diverge, the system leaves the instability band and regains control although the system stays 17 degree angle of attack since there is no damping. For a real vehicle, the ramping rate should likely be increased so that the angle of attack stays below 5 degrees after the rolling coupling instability band.

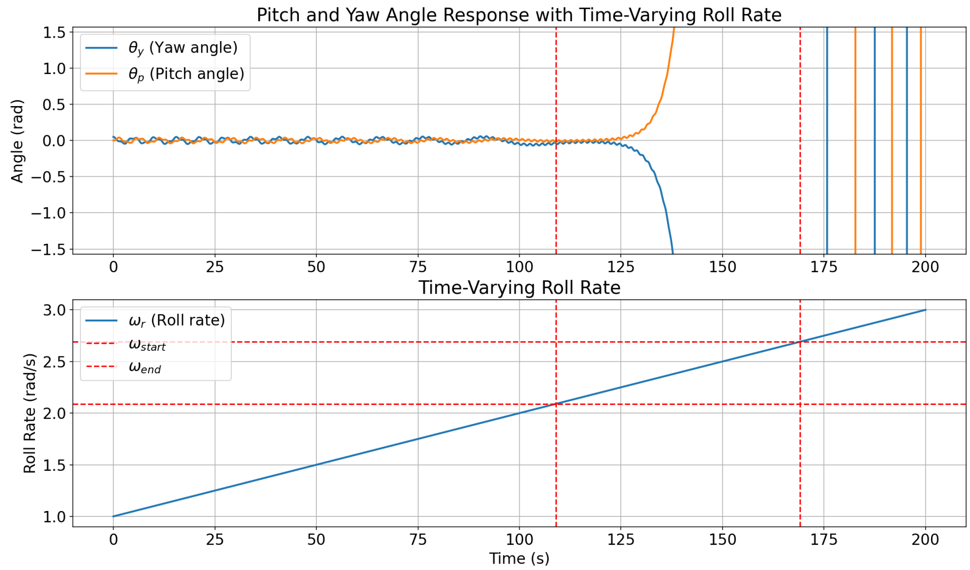

Fig. 3 Pitch and Yaw for slow roll rate ramping $\omega_r = 0.01t + 1$. This uses the same parameters as Fig. 2.

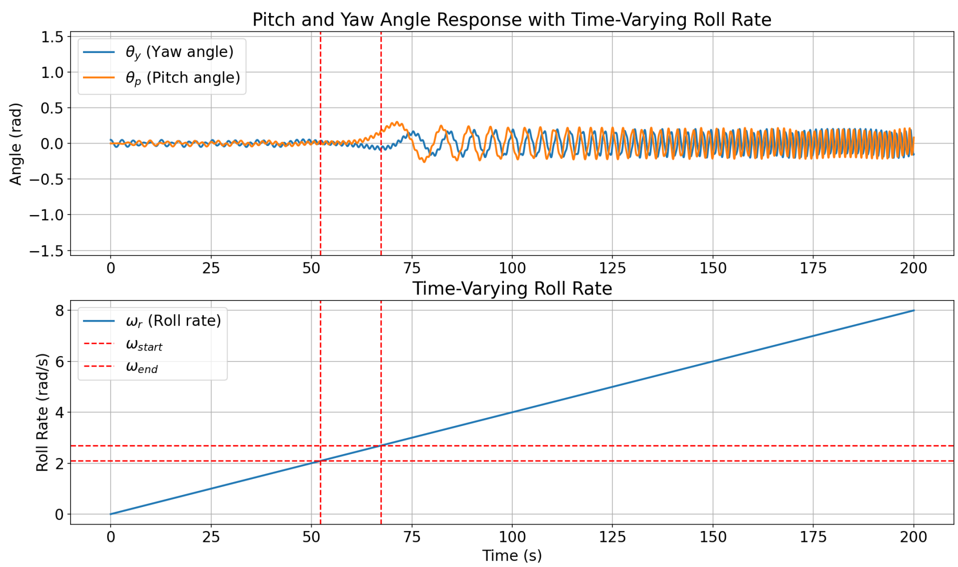

Fig. 4 Pitch and Yaw for fast roll rate ramping $\omega_r = 0.04t$. This uses the same parameters as Fig. 2.

V. Comparison of Roll Coupling Models for *Mach 'N' Roll*

Figs. 5 and 6 is a comparison of roll coupling frequency profile for GTXR's vehicle Mach 'N' Roll, a two-stage spin-stabilized sounding rocket scheduled to launch in summer 2026, using the different roll coupling models. The predicted pitch natural frequencies between the Mandell, LaBudde-Fetter, and RCDE models are within 2% error at worst. The LaBudde-Fetter models is very similar to the Mandell model since LaBudde and Fetter extend Mandell's derivation. The damping ratio for the LaBudde-Fetter model is higher due to the lateral movement of the rocket while the rocket corrects the non-zero angle of attack.

The RCDE model considers the roll rate coupling term between the second order ODEs unlike Mandell and LaBudde's derivations. This is why the dynamics for the RCDE model is a fourth order system as compared to the second order system literature models. If $k_y = k_p$ and $I_y = I_p$, $\omega_{start} = \omega_{end}$. Thus, pitch-yaw asymmetry is a requirement for an instability band to exist. A greater asymmetry leads to a more powerful roll coupling interaction in the instability band.

Though the various roll modeling models are similar, the models focus on different aspects of the rotational dynamics of a spin-stabilized rocket. By decoupling the pitch and yaw motions, the Mandell model explains the pitch and yaw rotational motion as two independent second order systems. The LaBudde-Fetter model extends the Mandell model by coupling the linear and rotational dynamics. Thus, the Mandell and LaBudde-Fetter models model the pitch and yaw dynamical response from a small perturbation well especially when $\omega_z \approx 0$ and thus the pitch-yaw coupling is negligible. The RCDE model focuses on the pitch-yaw coupling as the gyroscopic modal interaction leads to inertial roll coupling in spin-stabilized rockets, but uses a simpler aerodynamic model than the literature models.

The models predict similar frequencies since they both determine the system's natural resonance, but the mechanisms that amplifies these perturbations are different. For the literature models, the resonance amplification comes from the natural frequency of the second order system along the pitch or yaw axes. For the RCDE model, at resonance, the pitch-yaw coupling causes an initial perturbation on the pitch axis to induce a perturbation on the yaw axis at the system natural frequency leading to disturbance amplification. Therefore, a model that combines the more sophisticated aerodynamics from the literature models and the pitch-yaw coupling from the RCDE model would more completely represent the rotational dynamics for a spin-stabilized sounding rocket.

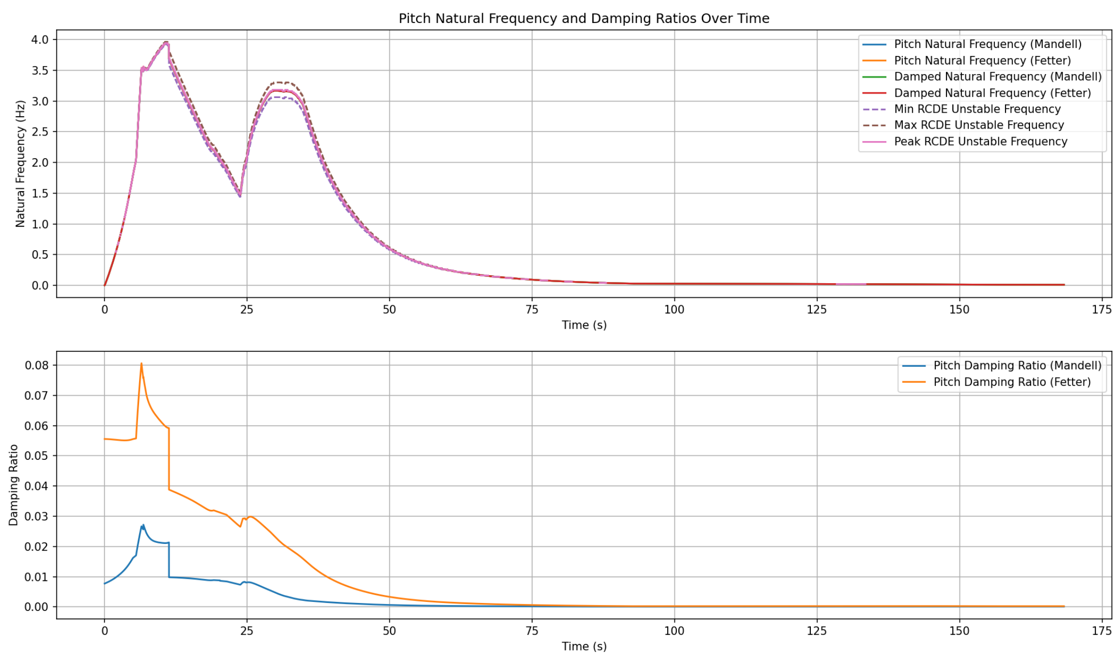

Fig. 5 Pitch natural frequencies and damping ratios over time for the Mandell, LaBudde-Fetter, and RCDE models for GTXR's Mach 'N' Roll vehicle. The blue, orange, green, red, and pink lines on the top graph are nearly identical.

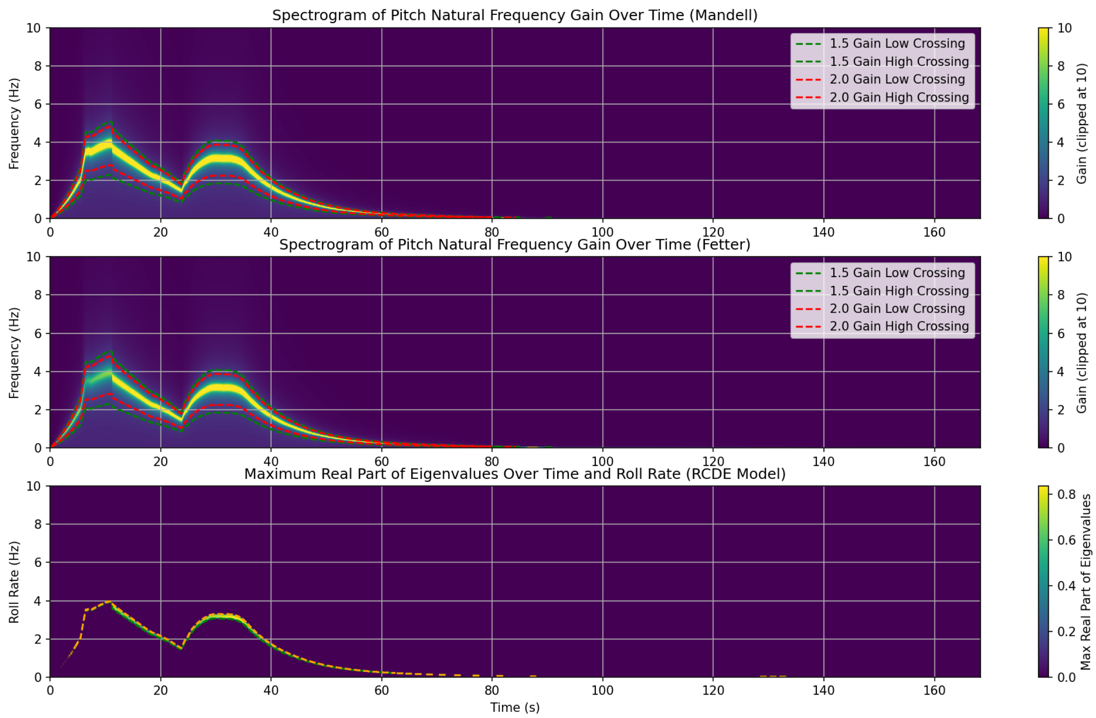

Fig. 6 Spectrogram of pitch natural frequencies over time for the Mandell, LaBudde-Fetter, and RCDE models for GTXR's Mach 'N' Roll vehicle.

VI. Conclusion

This paper demonstrates that while classical second-order rocket stability models accurately predict natural frequency trends, they omit direct pitch–yaw inertial coupling that becomes significant for spin-stabilized vehicles. The proposed RCDE model reveals a bounded roll-rate instability region driven by gyroscopic modal interaction, with instability occurring when roll rate approaches the vehicle's lateral natural frequency and when pitch–yaw asymmetry is present. Integrating the more thorough aerodynamics from literature models with the inertial coupling captured in the RCDE model would provide a more complete representation of rotational dynamics for high-speed, spin-stabilized sounding rockets.

Acknowledgments

The author thanks the Student Government Association at Georgia Tech and the Daniel Guggenheim School of Aerospace Engineering for logistically and financially supporting RRC. The author also thanks RRC's additional financial sponsors who contribute to the success of the team.

References

[1] Mandell, G. K., Caporaso, G. J., and Bengen, W. P., *Topics in Advanced Model Rocketry*, MIT Press, Cambridge, MA, 1973. Chapter 14: Rotational Dynamics. Available at: `https://www.scribd.com/document/918907773/Topics-in-Advanced-Model-Rocketry`.

[2] LaBudde, R. A., "A Design Procedure for Maximizing Altitude Performance," *Proceedings of the NARAM-41 Research and Development (R&D) Competition*, National Association of Rocketry (NAR), 1999. Available at: `https://www.apogeerockets.com/software/naram99.pdf`.

[3] Fetter, T. B., "Rotational Dynamic Stability," Technical Report Revision 1.2, Speedmotion Rockets, 2024. URL `http://www.speedmotionrockets.com/Rotational%20Dynamic%20Stability%20-%20Rev%201_2.pdf`.